Spectrochimica Acta Part B: Atomic Spectroscopy 187 (2022) 106342

Contents lists available at ScienceDirect

Spectrochimica Acta Part B: Atomic Spectroscopy

journal homepage: www.elsevier.com/locate/sab

# Towards airborne laser-induced breakdown spectroscopy: A signal recovery method for LIBS instruments subjected to vibrations

Santiago Palanco *, Sergio Aranda, Francisco Mancebo, María Cruz López-Escalante, Dietmar Leinen, José R. Ramos-Barrado

*Universidad de Málaga, Andalucía Tech, Departamento de Física Aplicada I, Campus de Teatinos, s/n, Málaga, 29071, Spain*

ARTICLE INFO

*Keywords:*
LIBS
Laser-induced breakdown spectroscopy
Stand-off
Remote
Drone
UAV
Unmanned aerial vehicle
Airborne

ABSTRACT

Sample or instrument vibrations can scatter laser impacts across the sample surface, which increases the uncertainty of laser-induced breakdown spectroscopy (LIBS) measurements. The common sources of noise associated to mechanical vibration are described and a method for isolating LIBS measurements from artifacts introduced by such fluctuations is presented. The approach circumvents the use of mechanical stabilizers by leveraging simple components common in LIBS systems. A camera was used to capture close-up images of the sample for each laser shot and the laser spot position in the sample surface was measured using common image processing techniques. By associating spectra with spatial coordinates in the sample surface, it was possible to reduce the relative standard deviation of the Cu(I) 427.51 nm signal in a patterned Cu/Al sample from 122.0% to 53.31%, similar to that measured for a pure Cu sample in the same vibration conditions. The spatial resolution of the method was found to depend on the laser spot diameter, the illuminance at the sample, the camera sensitivity and trigger insertion delay, and the speed of the laser beam sweeping the sample surface. The spatial resolution obtained with the setup used was ±0.6 mm at 15 m, i.e., 40 μm per meter of separation between the instrument and the sample with a vibration speed limit of 12 cm·s$^{-1}$.

## 1. Introduction

The development of instrumentation and methods for stand-off laser-induced breakdown spectroscopy carried out during the 2000s [1–4] demonstrated the suitability of laser-induced breakdown spectroscopy (LIBS) for remote analysis of composition, its applicability in hostile environments [5–10] the possibility of remote mapping of contaminated surfaces [11] and eventually, the ability for the in-situ detection of energetic compounds by mapping the surfaces of standoff vehicles [12]. In the context of insecurity caused by the terrorist attacks of that decade, the success of the latter test led to multimillion research programs on both sides of the Atlantic. Over ten demonstrators were built in less than five years and a range of configurations were explored, ranging from systems based on a single nanosecond laser source or those involving two nanosecond lasers [13,14] to a combination of a nanosecond laser followed by a microsecond or a millisecond re-excitation source [15–19].

In retrospect, it is striking that all these efforts have not evolved into commercial stand-off instruments. It could be argued that cost was an important issue in the next decade, marked by an economic downturn, still budget would be a minor factor for high-value applications. But along with the quest for greater sensitivity and working ranges, the instruments grew in complexity, size, and weight (~600 Kg) lacking the portability desirable on a field instrument. This fact could have been detrimental to a wider application. Not in vain, the Chemcam and SuperCam aboard the Curiosity and Perseverance Mars rovers [20,21] are the only instruments in operation today. For obvious reasons, their design followed the low-footprint design route like other instruments of the time [22–28].

The portability of a stand-off LIBS system can be largely improved with weight under 3 kg in a volume of less than 3000 cm$^3$ -a shoe box- including batteries for power supply. But to this end, the stand-off concept must be revised. Currently, there are air-cooled compact lasers commercially available but they provide lower pulse energy and beam quality as compared to the Nd:YAG sources in the above-mentioned demonstrators. In combination with the necessarily smaller focusing optics, the larger spot size at a given range yields a weaker plasma. Also, the smaller return optics gather less photons to a non-

* Corresponding author.
*E-mail address:* spalanco@uma.es (S. Palanco).

https://doi.org/10.1016/j.sab.2021.106342
Received 23 August 2021; Received in revised form 22 November 2021; Accepted 24 November 2021
Available online 27 November 2021

intensified detector, yielding lower signal-to-noise ratios. The affordable working range (5–15 m) is no longer in the hundreds of meters but the huge gains in portability make it possible to transport the instrument closer to the sample location aboard an unmanned aerial vehicle (UAV) [29] and reach targets otherwise unreachable even for man-portable instruments.

But in spite of this apparently logical evolution of the technology, the authors are not aware that another instrument of this kind have been built to date. As in many other techniques, multiple-shot signal accumulation or averaging is used in LIBS to improve the signal-to-noise ratio. An airborne instrument is specially affected by flight stability even under ideal steady conditions and, far from reducing the measurement uncertainty, averaging may have the undesired effect of convoluting information from different points as the laser wanders the sample surface. Even at the expense of adding undesired extra weight and complexity to the system, active stabilization systems are not of much help in mitigating these fluctuations. The best precision available from current commercial systems is ±0.03°, which proves insufficient as it translates into a residual error of 1 mm on the sample surface for each meter of separation between the instrument and the sample. Bear in mind that the span of the UAV alone takes up almost 1 m and that an additional safe operating distance of 3 to 5 m is required to avoid the turbulence returning from nearby surfaces.

In this paper we present a method for isolating spectral measurements from artifacts introduced by mechanical vibrations. The approach circumvents the use of mechanical stabilizers by leveraging simple components common in LIBS systems along with data analysis to enable the acquisition of a series of spectra from a given sample point when the instrument or the sample are subjected to vibrations.

## 2. Experimental setup

A simple stand-off LIBS instrument was built from stock components. Fig. 1-a shows a schematic diagram. A Nd: YAG laser source emitting 6 ns, 100 mJ pulses at a 10 Hz repetition rate was focused with a beam expander to a 1.1-mm spot on a sample separated 15 m from the instrument. A fraction of the optical emission of the resulting plasma was gathered with a commercial telescope (Omegon N150/750-EQ-3 F/5) which was mounted coaxially with the focusing beam expander. The telescope output was coupled to the input slit of an Andor Technology SR193i crossed Czerny-Turner spectrometer (1800 $l{\cdot}mm^{-1}$ grating) equipped with an Andor Technology DH720–18-F03 iCCD detector (spectral resolution: 0.04 $nm{\cdot}pixel^{-1}$) synchronized with the laser pulse output (gate delay and length: 850 ns, 1000 ns, respectively) which also triggered an IDS UI-3240-ML monochrome CMOS camera used to capture close-up images of the sample surface.

In order to reproduce the wander of a laser beam emitted from an airborne LIBS instrument on the surface of a distant sample, the sample holder (Fig. 1-b) was mounted to a custom-made device capable to provide adjustable repetitive in-plane trajectories while adding a certain degree of randomness both to position and speed. The sample holder was spring-loaded within a stationary frame. In-plain oscillations were induced by a spinning mechanical actuator with adjustable angular frequency and amplitude. Additional control of the oscillations could be achieved with a set of springs of various degrees of stiffness. The mass of the sample was 1.7% that of the holder.

## 3. Samples

Three metallic samples were used in this work, namely samples S1 to S3. S1 was an Al—Mg1.5 cast aluminum plate (Al > 96.6%, Cu < 0.2% w/w). S2 was a 0.5-mm-thick copper foil (Cu 99.98% w/w) which was glued to a rigid plastic holder for the ease of handling. S3 consisted of six square-shaped Cu pieces (same composition as S2) glued to the surface

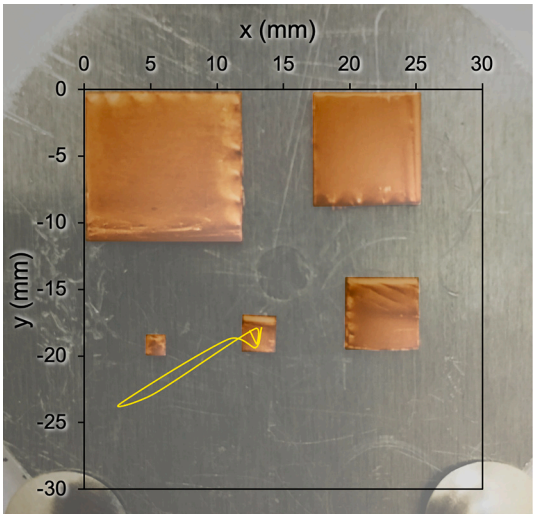


**Fig. 2.** Photograph of sample S3 showing the pattern of Cu squares glued to the base Al plate. For the present work only the two smaller Cu squares (1.5 and 2.5 mm were used). The yellow line overlay illustrates the base trajectory set with the sample holder for Figs. 3 and 4. The image has been digitally processed to improve edge detection. (For interpretation of the references to colour in this figure legend, the reader is referred to the web version of this article.)

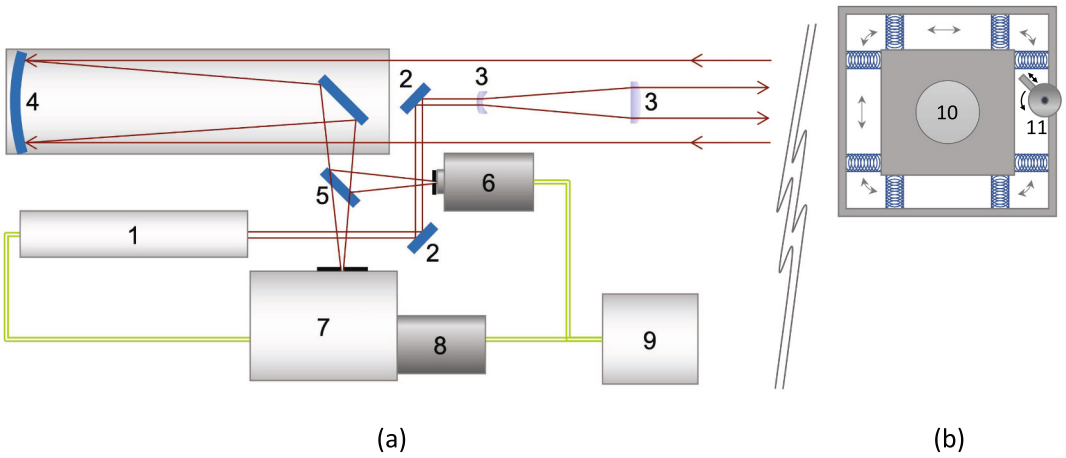


**Fig. 1.** Diagrams of: a) the stand-off LIBS instrument and b) the sample holder device. 1) laser head, 2) folding mirror, 3) focusing beam expander, 4) light collecting telescope, 5) splitter, 6) CMOS camera, 7) spectrograph, 8) iCCD detector, 9) computer, 10) sample holder, 11) motorized mechanical actuator.

of an aluminum plate (same composition as S1) and arranged as illustrated in Fig. 2.

## 4. Results and discussion

### 4.1. Mechanical vibrations as an error source

The three samples (S1, S2 and S3) were subjected to bidimensional oscillations in a plane perpendicular to the laser beam. The overlay in Fig. 2 shows the base trajectory set with the sample holder. Series of 150 shots were fired and both the spectrum and the sample image were acquired for each laser shot. Fig. 3-a shows the average spectrum of the 150 laser shots on sample S3. For comparison purposes, the same experiment was run with samples S1 (aluminum) and S2 (copper). Their corresponding spectra are shown in Figs. 3-b and 3-c, respectively. Except for a small contribution of the 402.26 nm, 406.26 nm and 427.51 nm Cu(I) lines, the spectrum in Fig. 3-a is very similar to that of aluminum in Fig. 3-b, the two prominent Al(I) lines at 394.40 nm and 396.15 nm being the most apparent features. Fig. 4 compiles the information extracted from several runs of 150 laser shots with the same experimental conditions. The relative standard deviation (RSD) of the background-subtracted Al(I) 396.15 nm and Cu(I) 427.51 nm signals is plotted versus the number of spectra averaged for each of the three samples. Five series have been included for S1 and S2 in order to compare the variability of the signal both within a series of spectra and across separate ones. As shown, the RSD for S3 signals is higher than those for the pure samples (41–71% vs 14–58% for Al(I) 396.15 nm, and 116–165% vs 37–71% for Cu(I) 427.51 nm).

On the other hand, no gains are obtained from averaging more than 10–15 shots for S1 and S2, while it seems pointless for S3. Moreover, sharp step-like changes can be observed in the four graphs. This effect is even more pronounced when the RSD is plotted as a 10-point boxcar sliding across the 150 spectra of each series (Figs. 4-e and 4-g for S1 and S2, respectively, and Figs. 4-f and 4-h for S3). This behavior is sourced in signal spikes and dips caused by the sampling spot wandering through fresh sample surface and that previously hit by the laser. A similar result was previously reported to occur during the operation of a hand-held probe. The instabilities induced by the operator's pulse shaking disappeared when the sample was held static against the probe [24]. Overall, the RSD in both S3 plots is higher than for their S1 and S2 counterparts. This was attributed to the heterogeneity of S3, which increases the variability of the signal since the laser beam alternates between Cu and Al along its trajectory through the surface. The RSD plots of the 10-point boxcar for S3, higher than their counterparts for S1 and S2, support this reasoning and, in fact, the fluctuations in Figs. 4-f and 4-h have well defined frequencies which match the vibrations induced by the sample holder, unlike with S1 and S2.

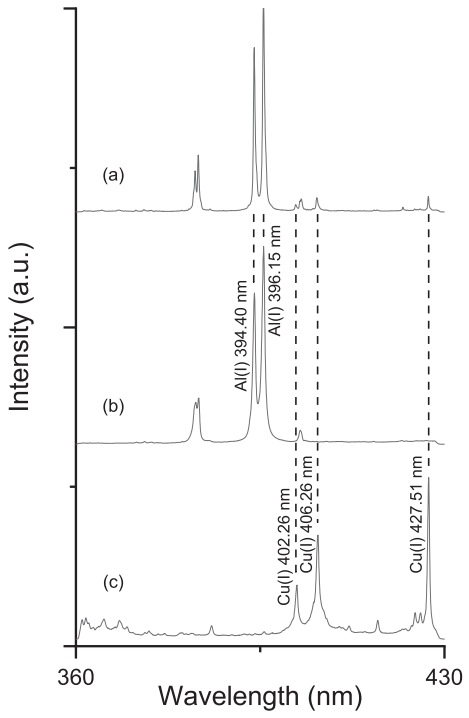


**Fig. 3.** Average of 150 LIBS spectra acquired at 15 m from the sample while subjected to the motion described in Fig. 2. a) Average spectrum of sample S3, b) average spectrum of sample S1, c) average spectrum of Sample S2.

### 4.2. Sample image as an additional information source

The above results describe the impact of vibrations on a stand-off LIBS system like those caused by wind or by an operator moving in the proximity of the instrument. Aiming to mitigate these effects, we explored adding the image of the sample surface as a second channel of information which, ideally, would allow to relate each spectrum to the spatial coordinates of its corresponding laser spot without an excessive extra weight. The only additional components required are a camera in sync with the laser pulse and simple optics. The spot coordinates are then calculated by processing its associated image. The capabilities of LIBS for chemical mapping are well known. Back in the 90s, researchers from Laserna's Group did extensive work on the subject [[30] and refs. therein]. The usual outcome of LIBS mapping is a raster image rendered by plotting the analysis results versus the corresponding spatial coordinates of each laser impact which is precisely set in the sample using micrometric stages.

In the absence of any positioning control over the sample or precise laser aiming, the approach presented here departs from the conventional method in the following aspects: i) the sample and/or the instrument are assumed to be in motion; ii) instead of precisely setting the sample position, the erratic instrument motion is leveraged to scan the sample surface, which implies iii) that some parts of the surface may not get to be analyzed and iv) that the spot coordinates have to be estimated from a photograph of the target at the instant of plasma formation and, as a consequence, v) the error associated to the spot position is not negligible. The latter has a direct impact in the analytical results and thus it was studied along with the main variables involved.

In the present case, the position measurement uses a combination of edge detection and other well-known pattern recognition techniques [31,32] which rely on the quality of the image captured. In turn, the latter depends on: (i) the ability of the lens and sensor to transfer resolution and contrast from the still sample, plus (ii) the ability of the setup to capture a still image from a target in motion. For this set of experiments, sample S3 was subjected to a bidimensional semi-random motion with the base trajectory shown in Fig. 5. The figure also includes a colour map and the actual distribution of the speed vector of the sample holder during the whole run. Fig. 6 features six maps of laser shots obtained with this type of motion under an illumination of $3{\cdot}10^3$ lx (corresponding to diffuse skylight) and camera exposure times between 0.3 and 90 ms. A simple sorting algorithm based on the Cu(I) 427.51/Al(I) 396.15 nm ratio was used to determine the presence of Cu. The spots for which Cu was detected are marked in red colour in the maps in Fig. 6. In addition, regions of interest (ROI) with a square shape and sizes between 1 and 5 mm were defined concentrically to the 1.5 mm Cu square on the sample surface. For each of the ROI, there is a plot in Fig. 6 representing the RSD of the Cu(I) 427.51 nm signal of those laser shots within the corresponding ROI.

For a given optical setup, noise associated to signal and motion blur dominate image quality. This becomes apparent in the maps at the bottom of Fig. 6, which show a higher dispersion both at short and long exposure time, while the spot positions measured tend to converge to a definite trajectory for the map obtained at a 10 ms exposure time. In fact,

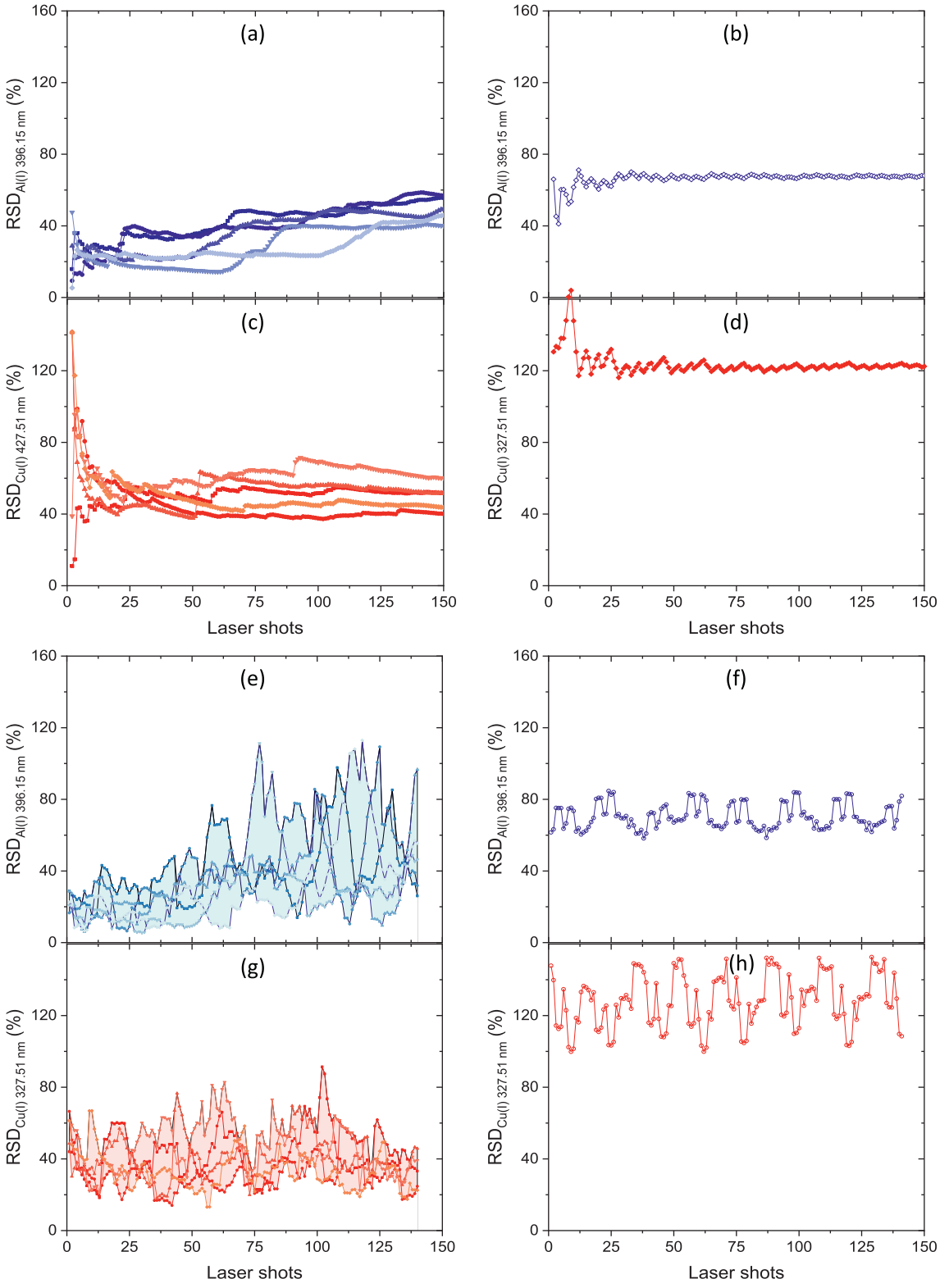


**Fig. 4.** Relative standard deviation (RSD) of the Al(I) 396,15 nm and the Cu(I) 327,51 nm signals for samples S1, S2 and S3. a) to d) RSD calculated for an increasing number of spectra starting from the first laser shot in the series and up to 150 shots averaged. Five data series corresponding to five separate experiments are shown for both S1 and S2 while only one series of sample S3 has been plotted for the sake of clarity. e) to h) RSD calculated for a ten-point boxcar moving across the same data as a) to d).

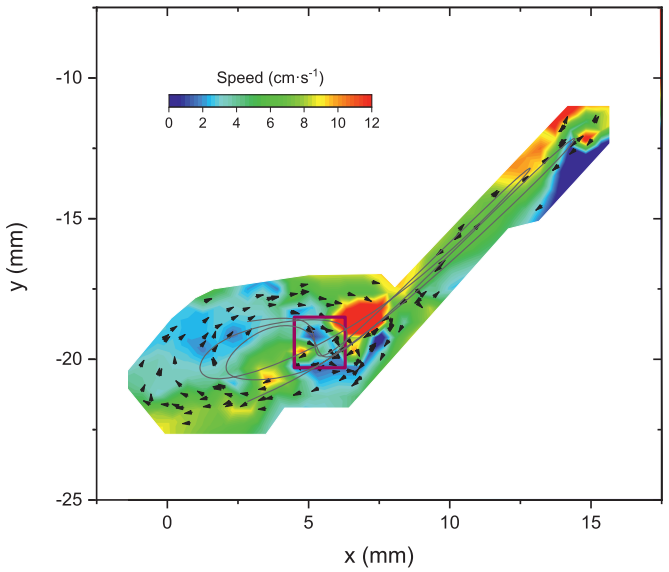


**Fig. 5.** (Solid line) base trajectory and distribution of speeds of the bidimensional semi-random motion applied to sample S3 for the experiments in Fig. 6. The red square marks the position of the copper feature in the sample surface. (For interpretation of the references to colour in this figure legend, the reader is referred to the web version of this article.)

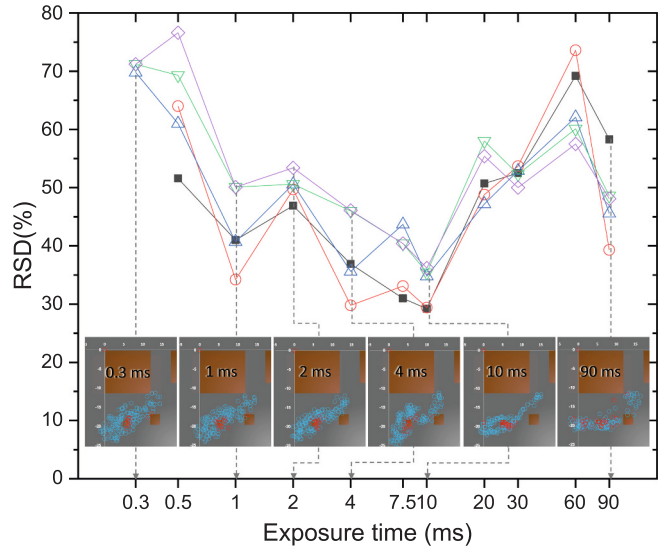


**Fig. 6.** (Bottom) maps of spots in sample S3 obtained with camera exposure times of 0.3, 1, 2, 4, 10 and 90 ms, and the motion illustrated in Fig. 5. Red circles denote laser spots where copper was detected and blue circles indicate spots where no Cu was detected. (Top) RSD of the Cu(I) 427.51 nm signal of those spots within a square ROI of (■) 1 mm, (○) 2 mm, (Δ) 3 mm, (▽) 4 mm and (◊) 5 mm. (For interpretation of the references to colour in this figure legend, the reader is referred to the web version of this article.)

for exposure times between 7,5 ms and 30 ms (not shown in Fig. 6 to avoid clutter), all the maps looked sharp to the naked eye. However, the RSD plots constrain the sharpest region to between 7,5 ms and 10 ms. At the low light levels involved in a stand-off LIBS setup, Fig. 6 illustrates the influence of camera sensitivity and exposure time on the ability of the method to produce precise results for the range of speeds studied. While at short exposure times, analytical uncertainty is driven by image noise, at long exposure times, motion blur becomes the dominant source of image quality degradation, leading to increased analytical uncertainty and, in turn, limiting the speed of the vibrations which can be effectively stabilized. For the setup and light levels used in this work, a 10 ms exposure was found to be the optimum setting for vibration speeds up to 12 cm·s$^{-1}$ at 15 m from the sample, which yielded a 35% RSD for the Cu(I) 427.51 nm signal. Although this result is significantly lower than that of Fig. 4-d and is indicative of the strength of the method, both figures are not directly comparable since the ROI considered and the trajectory are different on each case.

### 4.3. Actual performance of the method

The data acquired for Figs. 2 to 4 was used to assess the method. The spot positions during the experiment have been plotted in Fig. 7-a. Ten square ROI were defined concentrically to the 2.5-mm Cu square in order to estimate the spatial resolution of the method. Table 1 contains the dimensions of each ROI along with the number of laser spots which partially or fully overlapped the ROI, and the RSD of the Cu(I) 427.51 nm signal averaged from each ROI. For both, the number of spots and the RSD, separate columns have been provided detailing the total number of spots in the ROI and the number of those spots where Cu was detected. Also, the spectra averaged for the ROI of 1, 2, 3, 4, 8 and 23 mm have been plotted in Fig. 7-b. In contrast to the spectrum in Fig. 3-a, the spectra of the inner ROI in Fig. 7-b show a significant contribution of the Cu emission. The number of spots within the smallest 1-mm ROI is 32 and the RSD of the Cu(I) 427.51 nm signal is 61.15%, which is half that in Fig. 4-f and lays within the interval for sample S2 (Copper) in Fig. 4-c. It is worth noting that the Al emission is still present in the spectrum from the 1-mm ROI despite Cu was detected in all of the 32 spots. Due to the criterion followed to count the spots (those whose center point was within the ROI) the actual area analyzed is larger than the ROI by one spot diameter. For the larger ROI, the spot count increases and the RSD decreases to 53.31% and then remains constant (i.e., all Cu spots are contained within the 3-mm ROI). However, for the 2.5-mm ROI, the total point count and those with Cu differ. There are two Al-only points (this aspect was further checked with their corresponding spectra). The positioning error (0.5–0.6 mm) was eventually traced to a sporadic camera trigger insertion delay issue. Thus, taking this as a worst-case, it can be stated that the positioning error of the method is ±0.6 mm at 15 m for the current setup and experimental conditions, i.e., 40 μm per meter of separation between the instrument and the sample.

## 5. Conclusions

A method for isolating LIBS measurements from artifacts introduced by mechanical vibrations has been demonstrated. The approach circumvents the use of mechanical stabilizers by leveraging simple components common in LIBS systems. An inexpensive low-weight CMOS camera has proved sufficient to capture close-up images of the sample for each laser shot and the spot positions in the sample surface were measured with common image processing techniques. Sample or instrument vibrations have the effect of spreading the laser impacts across the sample increasing the uncertainty of LIBS measurements. The method tackles the problem from two angles: i) given an area of interest on the sample, undesired data obtained from other points in the sample can be filtered out, thus preventing the dilution of the analytical information into superfluous background. Then, relevant spectra can be either averaged together to improve the RSD or be used individually to gain spatially resolved information. Both approaches were demonstrated using a patterned Cu/Al sample. By associating spectra with spatial coordinates in the sample surface, it was possible to reduce the RSD of the Cu(I) 427.51 nm signal from 122.0% to 53.31%, a level which is similar to that measured for a pure Cu sample. This illustrates the potential of the method for the analysis of more complex samples with stand-off LIBS and airborne LIBS instruments. The spatial resolution of the method was found to depend on the laser spot diameter, the illuminance at the sample, the camera sensitivity and trigger insertion

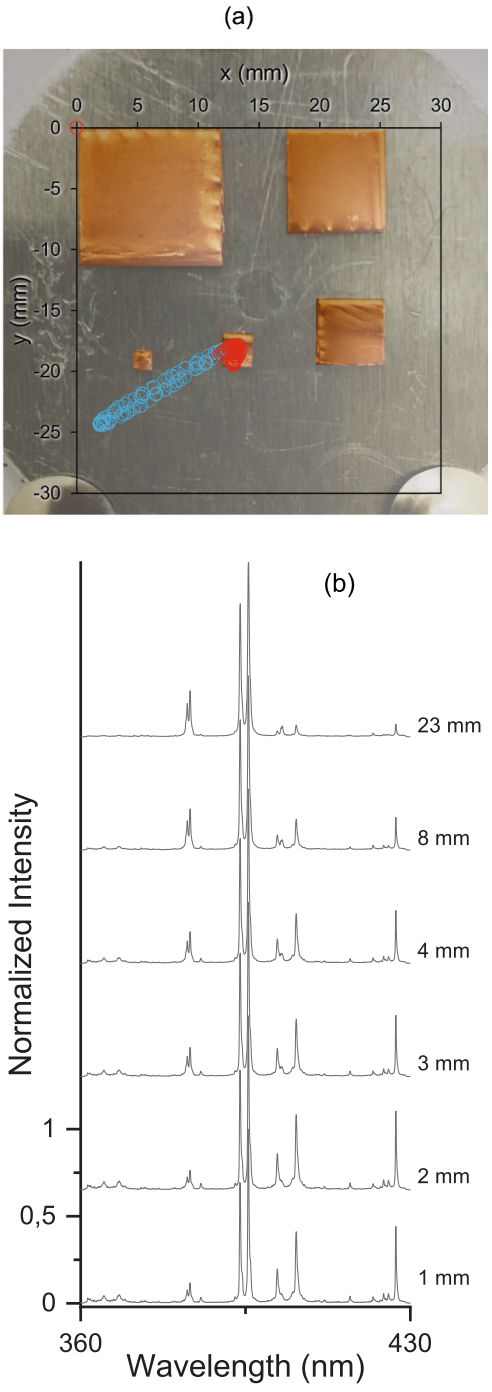


**Fig. 7.** a) Photograph of sample S3 with an overlay of the spots used for Fig. 4 (exposure time: 10 ms). Red circles denote spots where copper was detected. The image has been digitally processed to improve edge detection. b) LIBS spectra averaged for six concentric ROI (See Table 1 for further details). The six spectra have been normalized to the Al(I) 496.15 nm emission. (For interpretation of the references to colour in this figure legend, the reader is referred to the web version of this article.)

delay, and the intensity of the vibrations measured as the speed of the laser beam sweeping the sample surface. The spatial resolution obtained with the setup used was ±0.6 mm at 15 m, i.e., 40 μm per meter of separation between the instrument and the sample with a speed limit of 12 cm·s$^{-1}$. In the future, we plan to study the possibility to produce three-dimensional chemical maps by processing the information from overlapping spots, which in turn, could improve the surface sensitivity for the analysis of residues or layered materials.

**Table 1**
Dimensions of the ROI in Fig. 7-b. A separate column for both the spot count and the RSD of the Cu(I) 427.51 nm signal has been added to account for those spots which tested positive to Cu.

| ROI dimensions (mm) | | Number of spots in the ROI | | RSD (%) | |
|---|---|---|---|---|---|
| x | y | Total | With Cu | Total | With Cu |
| 1.0 | 1.0 | 32 | 32 | 61.15 | 61.15 |
| 1.5 | 1.5 | 39 | 39 | 58.19 | 58.19 |
| 2.0 | 2.0 | 49 | 49 | 57.88 | 57.88 |
| 2.5 | 2.5 | 61 | 59 | 58.70 | 55.80 |
| 3.0 | 3.0 | 70 | 66 | 58.70 | 53.31 |
| 3.5 | 3.5 | 72 | 66 | 61.22 | 53.31 |
| 4.0 | 4.0 | 73 | 66 | 62.49 | 53.31 |
| 5.0 | 5.0 | 76 | 66 | 66.18 | 53.31 |
| 8.0 | 8.0 | 85 | 66 | 76.18 | 53.31 |
| 23.0 | 23.0 | 150 | 66 | 122.0 | 53.31 |

## Declaration of Competing Interest

The authors declare that they have no known competing financial interests or personal relationships that could have appeared to influence the work reported in this paper.

## Acknowledgements

The authors would like to express their gratitude to Carlos Malagón of Astroshop (Málaga, Spain) for donating the telescope used in the stand-off LIBS instrument. This work has been partially supported by the Programa Estatal para la Incorporación Estable de Doctores (IEDI-2017-00828) and by the I Plan Propio de Investigación de la Universidad de Málaga (Spain). Funding for open access charge: Universidad de Málaga/CBUA.

## References

[1] David A. Cremers, Monty J. Ferris, Clara Y. Han, J.D. Blacic, Donald R. Pettit, Remote Elemental Analysis using Laser-induced Breakdown Spectroscopy, 1995, https://doi.org/10.1117/12.206450.
[2] S. Palanco, J.M. Baena, J.J. Laserna, Open-path laser-induced plasma spectrometry for remote analytical measurements on solid surfaces, Spectrochim. Acta Part B-Atomic Spectrosc. 57 (2002) 591–599. Pii s0584-8547(01)00388-3, https://doi.org/10.1016/s0584-8547(01)00388-3.
[3] S. Palanco, J. Laserna, Remote sensing instrument for solid samples based on open-path atomic emission spectrometry, Rev. Sci. Instrum. 75 (2004) 2068–2074, https://doi.org/10.1063/1.1753675.
[4] S. Palanco, C. Lopez-Moreno, J.J. Laserna, Design, construction and assessment of a field-deployable laser-induced breakdown spectrometer for remote elemental sensing, Spectrochim. Acta Part B-Atomic Spectrosc. 61 (2006) 88–95, https://doi.org/10.1016/j.sab.2005.12.004.
[5] A. Knight, N. Scherbarth, D. Cremers, M. Ferris, Characterization of laser-induced breakdown spectroscopy (LIBS) for application to space exploration, Appl. Spectrosc. 54 (2000) 331–340, https://doi.org/10.1366/0003702001949591.
[6] D.A. Cremers, R.C. Wiens, M.J. Ferris, J.D. Blacic, Development and testing of a prototype LIBS instrument for a NASA Mars rover, in: A. Sawchuk (Ed.), Laser Induced Plasma Spectroscopy and Applications, Optical Society of America, Orlando, Florida, 2002, https://doi.org/10.1364/LIBS.2002.ThE22 p. ThE22.
[7] D. Cremers, R. Wiens, M. Ferris, R. Brennetot, S. Maurice, Capabilities of LIBS for analysis of geological samples at stand-off distances in a Mars atmosphere, OSA Trends Optics Photon. Ser. 81 (2002), https://doi.org/10.1364/LIBS.2002.WA2.
[8] S. Palanco, S. Conesa, J.J. Laserna, Analytical control of liquid steel in an induction melting furnace using a remote laser induced plasma spectrometer, J. Anal. At. Spectrom. 19 (2004) 462–467, https://doi.org/10.1039/b400354c.
[9] B. Sallé, J.-L. Lacour, E. Vors, P. Fichet, S. Maurice, D. Cremers, R. Wiens, Laser-induced breakdown spectroscopy for Mars surface analysis: capabilities at stand-off distances and detection of chlorine and sulfur elements, Spectrochim. Acta B At. Spectrosc. 59 (2004) 1413–1422, https://doi.org/10.1016/j.sab.2004.06.006.
[10] C. Lopez-Moreno, S. Palanco, J.J. Laserna, Calibration transfer method for the quantitative analysis of high-temperature materials with stand-off laser-induced breakdown spectroscopy, J. Anal. At. Spectrom. 20 (2005) 1275–1279, https://doi.org/10.1039/b508528d.
[11] C. Lopez-Moreno, S. Palanco, J.J. Laserna, Remote laser-induced plasma spectrometry for elemental analysis of samples of environmental interest, J. Anal. At. Spectrom. 19 (2004) 1479–1484, https://doi.org/10.1039/b408534e.
[12] C. Lopez-Moreno, S. Palanco, J.J. Laserna, F. DeLucia, A.W. Miziolek, J. Rose, R. A. Walters, A.I. Whitehouse, Test of a stand-off laser-induced breakdown

spectroscopy sensor for the detection of explosive residues on solid surfaces, J. Anal. At. Spectrom. 21 (2006) 55–60, https://doi.org/10.1039/b508055j.
[13] J. Scaffidi, S.M. Angel, D.A. Cremers, Emission enhancement mechanisms in dual-pulse LIBS, Anal. Chem. 78 (2006) 24–32, https://doi.org/10.1021/ac069342z.
[14] V.I. Babushok, F.C. DeLucia, J.L. Gottfried, C.A. Munson, A.W. Miziolek, Double pulse laser ablation and plasma: laser induced breakdown spectroscopy signal enhancement, Spectrochim. Acta B At. Spectrosc. 61 (2006) 999–1014, https://doi.org/10.1016/j.sab.2006.09.003.
[15] D.K. Killinger, S.D. Allen, R.D. Waterbury, C. Stefano, E.L. Dottery, Enhancement of Nd:YAG LIBS emission of a remote target using a simultaneous CO2 laser pulse, Opt. Express 15 (2007) 12905–12915, https://doi.org/10.1364/OE.15.012905.
[16] A. Miziolek, P.C. Efthimion, Laser Assisted Microwave Plasma Spectroscopy, WO2008115287A2. https://patents.google.com/patent/WO2008115287A2/en, 2008.
[17] Y. Liu, M. Baudelet, M. Richardson, Elemental analysis by microwave-assisted laser-induced breakdown spectroscopy: evaluation on ceramics, J. Anal. At. Spectrom. 25 (2010) 1316–1323, https://doi.org/10.1039/C003304A.
[18] M. Weidman, S. Palanco, M. Baudelet, M.C. Richardson, Thermodynamic and spectroscopic properties of Nd:YAG-CO2 double-pulse laser-induced Iron plasmas, Spectrochim. Acta Part B-Atomic Spectrosc. 64 (2009) 961–967, https://doi.org/10.1016/j.sab.2009.07.023.
[19] M. Weidman, M. Baudelet, S. Palanco, M. Sigman, P.J. Dagdigian, M. Richardson, Nd:YAG-CO2 double-pulse laser induced breakdown spectroscopy of organic films, Opt. Express 18 (2010) 259–266, https://doi.org/10.1364/OE.18.000259.
[20] R.C. Wiens, S. Maurice, B. Barraclough, M. Saccoccio, W.C. Barkley, J.F. Bell, S. Bender, J. Bernardin, D. Blaney, J. Blank, M. Bouyé, N. Bridges, N. Bultman, P. Caïs, R.C. Clanton, B. Clark, S. Clegg, A. Cousin, D. Cremers, A. Cros, L. DeFlores, D. Delapp, R. Dingler, C. D'Uston, M. Darby Dyar, T. Elliott, D. Enemark, C. Fabre, M. Flores, O. Forni, O. Gasnault, T. Hale, C. Hays, K. Herkenhoff, E. Kan, L. Kirkland, D. Kouach, D. Landis, Y. Langevin, N. Lanza, F. LaRocca, J. Lasue, J. Latino, D. Limonadi, C. Lindensmith, C. Little, N. Mangold, G. Manhes, P. Mauchien, C. McKay, E. Miller, J. Mooney, R.V. Morris, L. Morrison, T. Nelson, H. Newsom, A. Ollila, M. Ott, L. Pares, R. Perez, F. Poitrasson, C. Provost, J. W. Reiter, T. Roberts, F. Romero, V. Sautter, S. Salazar, J.J. Simmonds, R. Stiglich, S. Storms, N. Striebig, J.-J. Thocaven, T. Trujillo, M. Ulibarri, D. Vaniman, N. Warner, R. Waterbury, R. Whitaker, J. Witt, B. Wong-Swanson, The ChemCam instrument suite on the Mars science laboratory (MSL) rover: body unit and combined system tests, Space Sci. Rev. 170 (2012) 167–227, https://doi.org/10.1007/s11214-012-9902-4.
[21] R.C. Wiens, S. Maurice, O. Gasnault, R.B. Anderson, O. Beyssac, L. Bonal, S. Clegg, L. Deflores, G. Dromart, W.W. Fischer, O. Forni, J.P. Grotzinger, J.R. Johnson, J. Martinez-Frias, N. Mangold, S. McLennan, F. Montmessin, F. Rull, S.K. Sharma, A. Cousin, P. Pilleri, V. Sautter, E. Lewin, E. Cloutis, F. Poulet, S. Bernard, T. McConnochie, N. Lanza, H. Newsom, A. Ollila, R. Leveille, S. Le Mouelic, J. Lasue, N. Melikechi, P.-Y. Meslin, O. Grasset, S.M. Angel, T. Fouchet, P. Beck, B. Bousquet, C. Fabre, P. Pinet, K. Benzerara, G. Montagnac, G. Arana, K. Castro, J. Laserna, J.M. Madariaga, J.-A. Manrique, G. Lopez, R. Lorenz, D. Mimoun, T. Acosta-Maeda, C. Alvarez, E. Dehouck, G. Delory, A. Doressoundiram, R. Francis, J. Frydenvang, T. Gabriel, X. Jacob, M.B. Madsen, J. Moros, N. Murdoch, R. Newell, J. Porter, C. Quantin-Nataf, W. Rapin, S. Schroeder, P. Sobron, M. Toplis, A.J. Brown, M. Veneranda, B. Chide, C. Legett, C. Royer, A. Stott, D. Vogt, S. Robinson, D. Delapp, E. Clave, S. Connell, A. Essunfeld, Z. Gallegos, C. Garcia-Florentino, E. Gibbons, J. Huidobro, E. Kelly, H. Kalucha, P. Ruiz, I. Torre-Fdez, S. Shkolyar, SuperCam Team, SuperCam on the Perseverance Rover for Exploration of Jezero Crater: Remote LIBS, VISIR, Raman, and Time-Resolved Luminescence Spectroscopies Plus Micro-Imaging and Acoustics, 2021, p. 1182. https://ui.adsabs.harvard.edu/abs/2021LPI....52.1182W.
[22] K.Y. Yamamoto, D.A. Cremers, M.J. Ferris, L.E. Foster, Detection of metals in the environment using a portable laser-induced breakdown spectroscopy instrument, Appl. Spectrosc., AS. 50 (1996) 222–233.
[23] B.C. Castle, A.K. Knight, K. Visser, B.W. Smith, J.D. Winefordner, Battery powered laser-induced plasma spectrometer for elemental determinations, J. Anal. At. Spectrom. 13 (1998) 589–595, https://doi.org/10.1039/A708844B.
[24] S. Palanco, A. Alises, J. Cunat, J. Baena, J.J. Laserna, Development of a portable laser-induced plasma spectrometer with fully-automated operation and quantitative analysis capabilities, J. Anal. At. Spectrom. 18 (2003) 933–938, https://doi.org/10.1039/b303248e.
[25] S. Palanco, J. Laserna, Spectral analysis of the acoustic emission of laser-produced plasmas, Appl. Opt. 42 (2003) 6078–6084, https://doi.org/10.1364/AO.42.006078.
[26] S. Conesa, S. Palanco, J.J. Laserna, Acoustic and optical emission during laser-induced plasma formation, Spectrochim. Acta Part B-Atomic. Spectrosc. 59 (2004) 1395–1401, https://doi.org/10.1016/j.sab.2004.06.004.
[27] B. Sallé, D. Cremers, S. Maurice, R. Wiens, P. Fichet, Evaluation of a compact spectrograph for in-situ and stand-off laser-induced breakdown spectroscopy analyses of geological samples on Mars missions, Spectrochim. Acta B At. Spectrosc. 60 (2005) 805–815, https://doi.org/10.1016/j.sab.2005.05.007.
[28] R.S. Harmon, F.C. DeLucia, C.E. McManus, N.J. McMillan, T.F. Jenkins, M. E. Walsh, A. Miziolek, Laser-induced breakdown spectroscopy – an emerging chemical sensor technology for real-time field-portable, geochemical, mineralogical, and environmental applications, Appl. Geochem. 21 (2006) 730–747, https://doi.org/10.1016/j.apgeochem.2006.02.003.
[29] Chemocopter. (n.d.). https://www.chemocopter.com/ (accessed August 11, 2021).
[30] J.M. Vadillo, J.J. Laserna, Laser-induced plasma spectrometry: truly a surface analytical tool, Spectrochim. Acta B At. Spectrosc. 59 (2004) 147–161, https://doi.org/10.1016/j.sab.2003.11.006.
[31] F.Y. Shih, Image Processing and Pattern Recognition: Fundamentals and Techniques, John Wiley & Sons, 2010.
[32] R. Chityala, S. Pudipeddi, Image Processing and Acquisition Using Python, Chapman & Hall/CRC Press, 2020. https://books.google.es/books?id=s05tzQEACAAJ.